

ARTICLE

Received 27 Oct 2015 | Accepted 15 Jun 2016 | Published 26 Jul 2016

DOI: 10.1038/ncomms12247

OPEN

# Sea ice and millennial-scale climate variability in the Nordic seas 90 kyr ago to present

Ulrike Hoff<sup>1</sup>, Tine L. Rasmussen<sup>1</sup>, Ruediger Stein<sup>2,3</sup>, Mohamed M. Ezat<sup>1,4</sup> & Kirsten Fahl<sup>2</sup>

In the light of rapidly diminishing sea ice cover in the Arctic during the present atmospheric warming, it is imperative to study the distribution of sea ice in the past in relation to rapid climate change. Here we focus on glacial millennial-scale climatic events (Dansgaard/Oeschger events) using the sea ice proxy IP<sub>25</sub> in combination with phytoplankton proxy data and quantification of diatom species in a record from the southeast Norwegian Sea. We demonstrate that expansion and retreat of sea ice varies consistently in pace with the rapid climate changes 90 kyr ago to present. Sea ice retreats abruptly at the start of warm interstadials, but spreads rapidly during cooling phases of the interstadials and becomes near perennial and perennial during cold stadials and Heinrich events, respectively. Low-salinity surface water and the sea ice edge spreads to the Greenland–Scotland Ridge, and during the largest Heinrich events, probably far into the Atlantic Ocean.

<sup>1</sup>CAGE—Centre for Arctic Gas Hydrate, Environment and Climate, Department of Geology, UiT, The Arctic University of Norway, NO-9037 Tromsø, Norway.

<sup>2</sup>Alfred Wegener Institute, Helmholtz Centre for Polar and Marine Research, D-27568 Bremerhaven, Germany. <sup>3</sup>Department of Geosciences (FB5), Klagenfurter Strasse 4, University of Bremen, 28359 Bremen, Germany. <sup>4</sup>Department of Geology, Faculty of Science, Beni-Suef University, Beni-Suef, Egypt. Correspondence and requests for materials should be addressed to U.H. (email: ulrike.hoff@uit.no).

Dansgaard/Oeschger (D/O) events in Greenland ice cores consist of warm interstadial (IS) and cold stadial events<sup>1</sup> and are strongly imprinted in sediments from the northern North Atlantic region and Nordic seas<sup>2,3</sup>. In general the warming to interstadial conditions was abrupt as seen in Greenland ice cores and marine records. The warm conditions were followed by gradual cooling called the interstadial transitional cooling phase, and a rapid transition to cold stadial conditions. Larger and/or longer-lasting stadials correlate with North Atlantic Heinrich events (H-events)<sup>2</sup>, where numerous icebergs were released from the Laurentide ice sheet and melting over the North Atlantic region in the so-called Ruddiman belt<sup>4,5</sup> (Fig. 1). Even though D/O events have been extensively studied, changes in sea ice cover have only been inferred by indirect evidence for presence or absence of sea ice (for example, deposition patterns of ice-rafted debris, oxygen isotope records and palaeo-temperature reconstructions) (Supplementary Fig. 1 and Supplementary Table 1).

The Nordic seas are characterized by northward inflow of warm, saline Atlantic surface Water (North Atlantic Current, Northwest Atlantic Current, North Atlantic surface Water, Faroe Current) and southward outflow of cold Polar surface Water (East Greenland Current and East Icelandic Current)<sup>6</sup>

(Fig. 1). In the Fram Strait, the Atlantic Water continues its flow below the sea ice-covered Polar surface Water as an intermediate water mass<sup>7</sup>. In the central part of the Nordic seas cooling and sinking of the salty surface water during the winter months generate cold deep overflows over the Greenland–Scotland Ridge into the North Atlantic<sup>6,7</sup>. The inflow of Atlantic surface Water is the major source of heat to the Arctic and Nordic seas, and it is generally agreed that changes in ocean circulation and sea ice cover has played a major role in the control of past millennial-scale climate changes of the glacial D/O events<sup>2,8,9</sup>.

The Atlantic surface Water is ice-free throughout the year, while the East Greenland Current is covered by drifting near-perennial sea ice. In the central parts of the Nordic seas, mixing of Atlantic Water with Polar Water forms the zone of Arctic surface Water, which is located between the Arctic and Polar fronts<sup>6</sup> (Fig. 1). The Arctic surface Water is seasonally sea ice covered and comprises the marginal ice zone (MIZ). The location of the MIZ and the Arctic and the Polar fronts changes with the seasons and on inter-annual and longer-time scales<sup>10</sup>. In the East Greenland Current behind the Polar front productivity is very low, while intermediate to high productivity is found in the ice-free zone of Atlantic surface Water. The highest seasonal

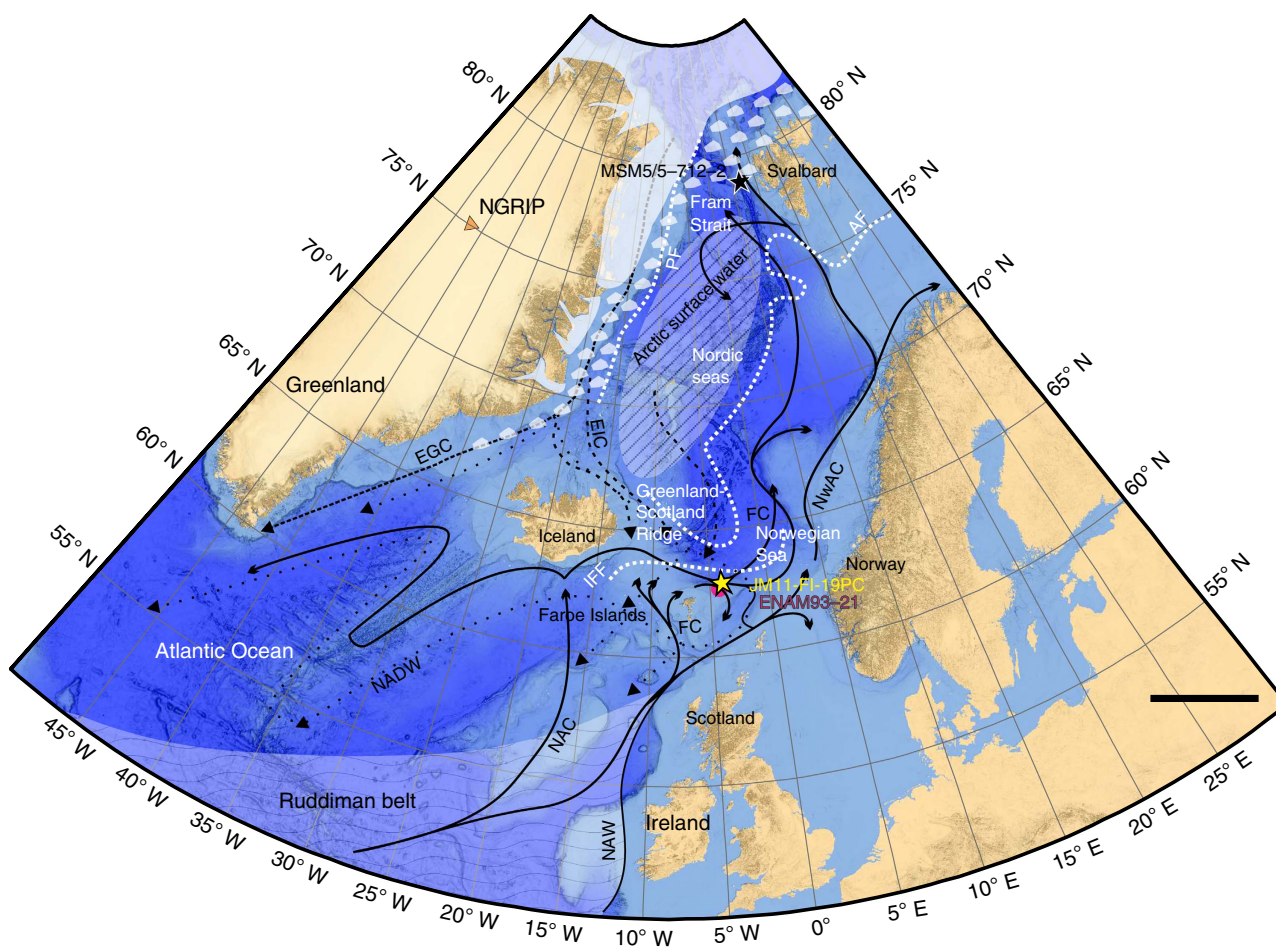


**Figure 1 | Map of the Nordic seas.** Location of studied sediment core JM11-FI-19PC (yellow star) along with nearby core ENAM93-21/MD95-2009 (refs 3,66–68) (magenta coloured circle) and core MSM5/5-712-2<sup>17</sup> (black star) from the Svalbard margin, discussed in the text, are marked. Bathymetry from GEBCO 2014 grid (<http://www.gebco.net/>). Major surface (solid and dashed black lines) and bottom currents (dotted black lines), locations of Arctic Front (AF) including the Iceland-Faroe front (IFF) and Polar Front (PF) (dashed white lines) are indicated together with the modern location of summer sea ice limit (shaded white area with drift ice), and the location of the Arctic surface water (shaded area with diagonal lines), as well as the Ruddiman belt (shaded area with wave-shaped lines). EGC, East Greenland Current; EIC, East Icelandic Current; FC, Faroe Current; NAC, North Atlantic Current; NADW, North Atlantic Deep Water; NAW, North Atlantic Water; NwAC, Northwest Atlantic Current; NGRIP, North Grip ice core (orange triangle). Scale bar, 500 km.

productivity occurs at the frontal areas and in the MIZ<sup>11,12</sup>. The positions of the Arctic and Polar fronts and the degree of sea ice cover thus depend on the distribution of the major surface water masses in the Nordic seas. A recent study showed that in the Arctic Ocean, the flow of Atlantic Water has a direct impact on sea ice distribution<sup>13</sup>.

Previous studies of a C<sub>25</sub> isoprenoid lipid (IP<sub>25</sub>) synthesized mainly by diatoms have shown its potential as a valuable new proxy for the reconstruction of the presence of seasonal sea ice<sup>14–19</sup>. IP<sub>25</sub> reportedly is produced by a few sea ice diatom species within the genera *Haslea* and *Pleurosigma*<sup>20</sup>. Furthermore, IP<sub>25</sub> is a stable organic compound preserved in sediments as old as Late Miocene and Pliocene<sup>21–23</sup>, and can be used in environments where other micropalaeontological sea ice proxies are absent or disturbed by dissolution effects<sup>14,24</sup>. Open-ocean conditions have been successfully reconstructed by using phytoplankton-derived sterols as a proxy for increased surface productivity such as brassicasterol and dinosterol<sup>15,25,26</sup>. The calculated ratio IP<sub>25</sub> to brassicasterol and dinosterol, the so-called P<sub>B</sub>IP<sub>25</sub> and P<sub>D</sub>IP<sub>25</sub>, respectively, can be related to sea ice coverage on a scale from permanent sea ice to year-round open water. In both ends of the scale, the IP<sub>25</sub> proxy is practically absent<sup>15,16,26</sup>, but accompanied by either low or high brassicasterol and dinosterol values, respectively<sup>26,27</sup>.

In this study we present results of IP<sub>25</sub>, brassicasterol, dinosterol, total organic carbon (%TOC) and δ<sup>13</sup>C<sub>org</sub>

(as terrigenous/marine organic-matter proxy; see ref. 28) together with the calculated sea ice indicators P<sub>B</sub>IP<sub>25</sub> and P<sub>D</sub>IP<sub>25</sub>, in the interval 801–2 cm of sediment core JM11-FI-19PC from the SE Norwegian Sea (see Methods and Fig. 1 for core location). In addition, low-resolution counts and identification of diatom frustules have been performed (see Methods). The purpose of this study is to reconstruct sea ice cover in the past in relation to millennial-scale climate change during the last 90 kyr in medium to high resolution. We compare our records with previously published records from the Fram Strait and published records that have provided indirect evidence for sea ice distribution and ocean circulation on millennial timescale from the northern North Atlantic (Fig. 1, Supplementary Fig. 1 and Supplementary Table 1). The chosen core site is from the northern Faroe Islands margin in the SE Norwegian Sea, close to the position of previously published core ENAM93-21/MD95-2009 (ref. 3). The site is close to the Iceland–Faroe Front (IFF) that marks the boundary between the cold East Icelandic Current branching off the East Greenland Current and the Faroe Current branch of the inflowing Atlantic surface Water<sup>6</sup> (Fig. 1). The northern Faroe margin is presently sea ice free year round, but historical records show that during the Little Ice Age sea ice drift reached to the Faroe Islands via the East Icelandic Current<sup>29</sup>.

Our study shows that the sea ice retreats abruptly at the start of warm Interstadials and spreads rapidly during cooling phases of the Interstadials, before it becomes near-perennial and perennial

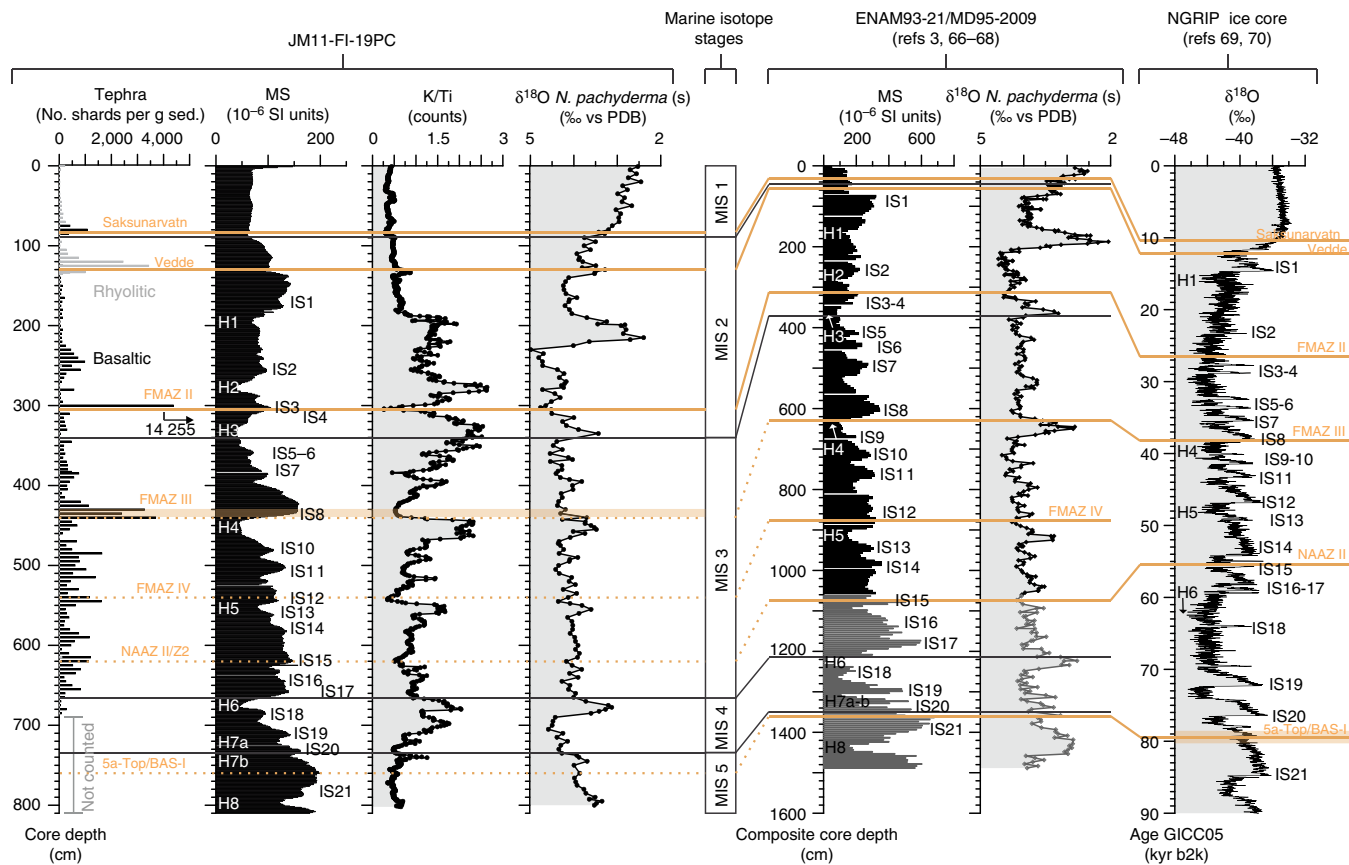


**Figure 2 | Stratigraphic correlation of JM11-FI-19PC to nearby marine core ENAM93-21/MD95-2009 and the NGRIP ice core.** Tephra layers are shown in orange (solid lines, used in age model calculations; dashed lines, not used in age model calculations; see explanations to Supplementary Table 2). Basaltic tephra counts for JM11-FI-19PC are shown in black bars, while rhyolitic tephra counts are shown in light grey bars. Orange shaded bar at the FMAZ III tephra from core JM11-FI-19PC indicate depth range of the tephra zone (see explanations to Supplementary Table 2). Orange shaded bar at the 5a-Top/BAS-I tephra layer in data from the NGRIP ice core indicates uncertainty in age for this tephra layer (see explanations to Supplementary Table 2). H, H-event; K/Ti, XRF measurement of the ratio between potassium and titanium; MS, Magnetic susceptibility; δ<sup>18</sup>O *N. pachyderma* s, planktic foraminiferal species. Data from sediment (sed.) cores ENAM93-21/MD95-2009 are from refs 3,66–68, while NGRIP ice core data are from refs 69,70.

during cold stadials and H-events, respectively. The distribution of sea ice correlates closely with climate and variations in ocean circulation, in flow of meltwater and stratification of the ocean surface.

## Results

**Correlation and age model.** The age model for the last 90 kyr interval of sediment core JM11-FI-19PC is based on well-known tephra layers (Figs 2 and 3 and Supplementary Table 2), 11 AMS- $^{14}\text{C}$  dates (Fig. 3 and Supplementary Table 3) and 20 magnetic susceptibility (MS), potassium/titanium (K/Ti) and  $\delta^{18}\text{O}$  tie points of interstadial onsets (Fig. 3 and Supplementary

Table 4). It has previously been demonstrated that the signal of MS and benthic  $\delta^{18}\text{O}$  values in marine records from the SE Nordic seas correlate closely in time with the (North) Greenland ice core  $\delta^{18}\text{O}$  signal<sup>3,30</sup> (Fig. 2). The characteristic saw-tooth pattern of the D/O events in the ice cores is recognized in the MS of our core (Fig. 2). High values correlate with interstadial and minimum values with stadial (S) climate, respectively. The presented interval of JM11-FI-19PC comprises the interstadials IS21–IS1 (IS1 = Bølling and Allerød interstadials<sup>1</sup>) and H-events H8–H1 (refs 8,31), which is equivalent to the last 90 kyr b2k (before year AD 2000) (Figs 2 and 3).

The age control of the core JM11-FI-19PC younger than 65 kyr b2k has been presented by Ezat *et al.*<sup>30</sup>, while the age model for the interval older than 65 kyr b2k is new (see Methods and Supplementary Information for details). Sample resolution in the studied interval 90 kyr ago to present (per 1-cm thick sample) varies between 35 and 320 years, while the sedimentation rates vary between 0.28 mm per year (Fig. 3).

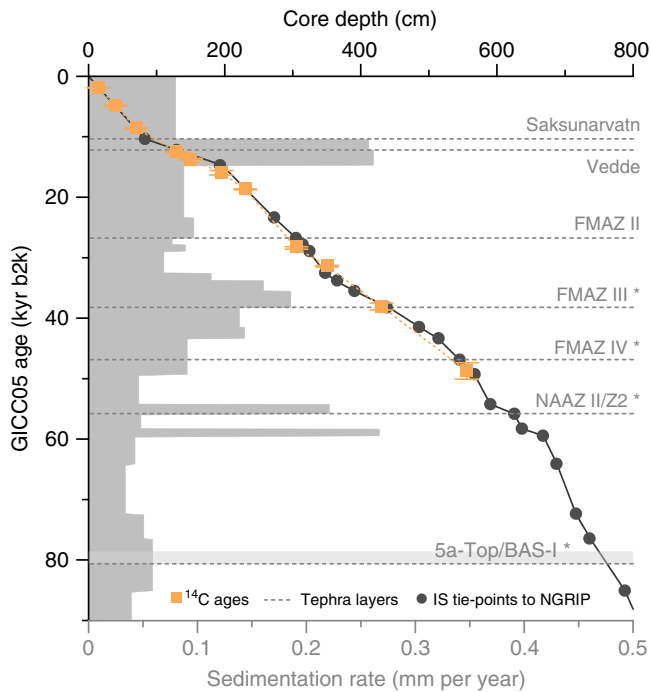


**Figure 3 | Age-depth relationship and sedimentation rates of the upper 801 cm of sediment core JM11-FI-19PC.** Tephra layers marked with \* (FMAZ III, IV, NAAZ II/Z2 and 5a-Top/BAS-I) have not been used in the calculations of the age model (see also Methods and explanations to Supplementary Table 2). Error bars are given in s.d.

**IP<sub>25</sub> and other biomarkers.** For the last 30,000 years, trends in our PIP<sub>25</sub> record are similar to core MSM5/5-712-2 from the western Svalbard margin (for core location see Fig. 1) with very similar IP<sub>25</sub>, P<sub>B</sub>IP<sub>25</sub> and P<sub>D</sub>IP<sub>25</sub> values<sup>17</sup> (Fig. 4). In the Svalbard record, maxima in sea ice cover occurred in marine isotope stage (MIS) 2 (between 30 and 17 kyr ago), while the sea ice cover was slightly reduced after 17 kyr ago in the warm Bølling and Allerød interstadials (IS1) and in the Holocene<sup>17</sup> (Fig. 4). A very similar development is seen at the northern Faroe margin and with the same events clearly marked. The similarity of the data indicates that the sea ice proxy results for the Faroe margin are overall reliable. The minor offsets in the timing of the IP<sub>25</sub>, to P<sub>B</sub>IP<sub>25</sub> and P<sub>D</sub>IP<sub>25</sub> might reflect uncertainties in the age models and the fact, that the Svalbard record is located in the direct flow of Atlantic Water, while JM11-FI-19PC is also influenced by the IFF (Fig. 1).

For the part older than 30 kyr, sea ice variability (reflected in the IP<sub>25</sub>, P<sub>B</sub>IP<sub>25</sub> and P<sub>D</sub>IP<sub>25</sub> records) and related short-term changes in surface-water productivity (reflected in the brassicasterol and dinosterol records and in the flux patterns of diatoms) seem to follow very clearly the D/O events (Fig. 5).

## Discussion

In late MIS 3 to early MIS 2 (c. 35–22 kyr ago), the interstadials of D/O events 6–2 are short-lasting, and because of the relatively low

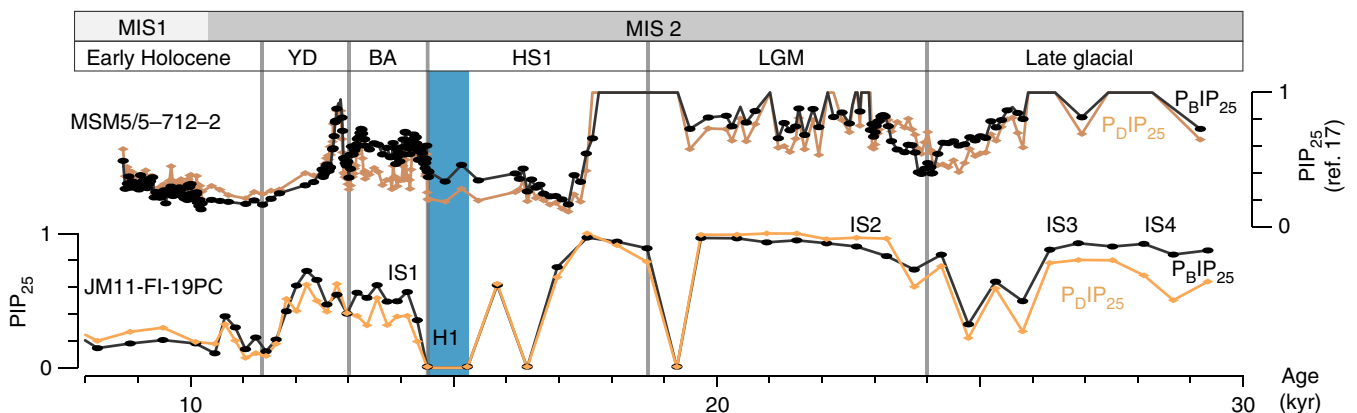


**Figure 4 | Sea ice proxies for the time interval between 30 and 8 kyr ago.** Comparison of P<sub>B</sub>IP<sub>25</sub> and P<sub>D</sub>IP<sub>25</sub> signals of sediment core JM11-FI-19PC (GICC05-timescale) and sediment core MSM5/5-712-2 (calibrated age scale) from the Svalbard margin published by Müller and Stein<sup>17</sup>. For H-event 1 (blue bar), characterized by IP<sub>25</sub> and brassicasterol (as well as dinosterol) values of close to or zero (that is, ‘zero divided by zero’), per definition maximum P<sub>B</sub>IP<sub>25</sub> and P<sub>D</sub>IP<sub>25</sub> values of 1 were assumed (for background see refs 15,26). For core locations, see Fig. 1. BA, Bølling and Allerød interstadial; H, H-event; HS, Heinrich stadial; LGM, Last Glacial maximum; YD, Younger Dryas.

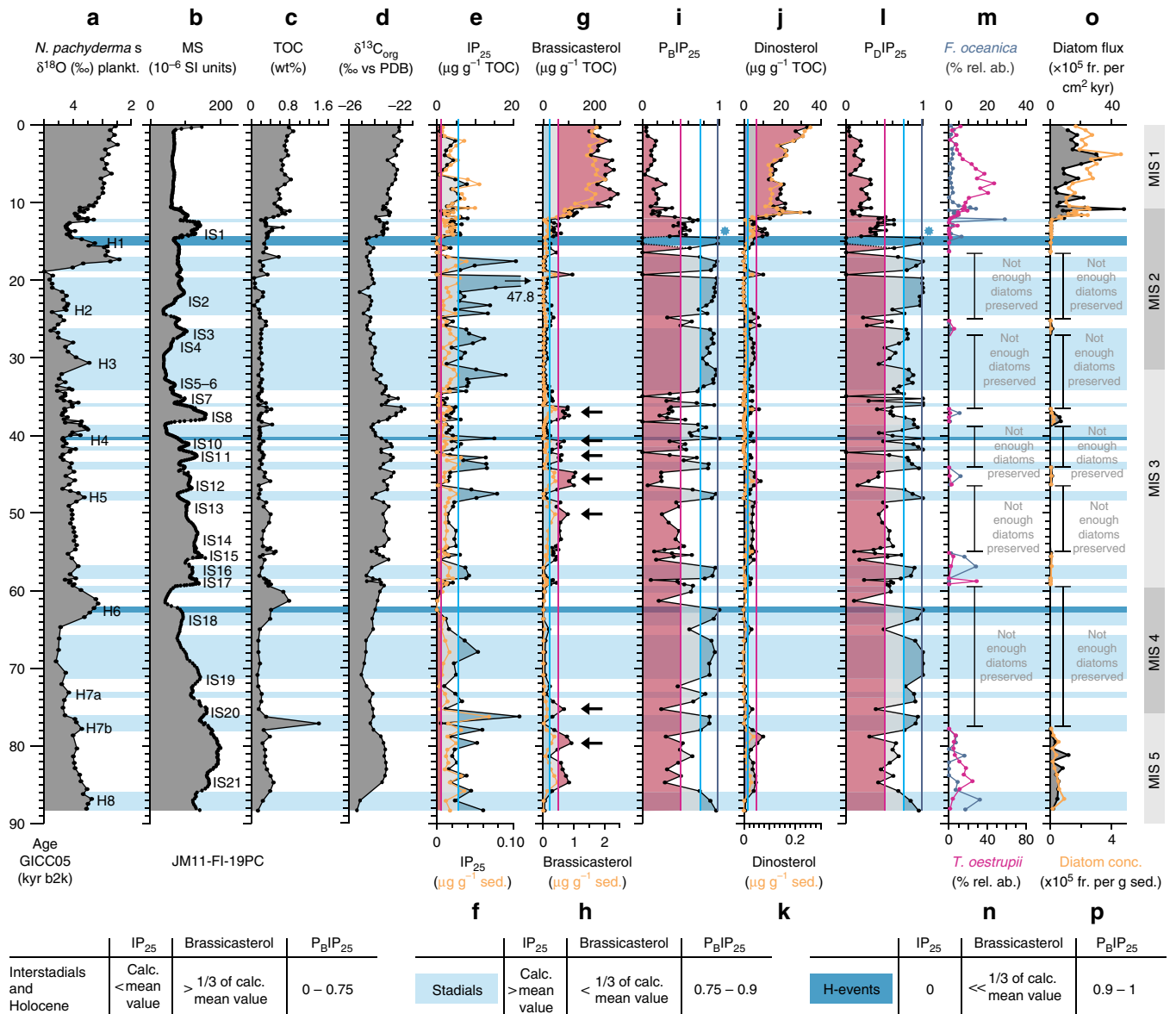


**Figure 5 | Proxy data of sediment core JM11-FI-19PC 90 kyr b2k to present.** (a)  $\delta^{18}\text{O}$  measured in planktic foraminiferal species *N. pachyderma* s (% versus (vs) Pee Dee Belemnite (PDB)), (b) MS ( $10^{-6}$  SI units), (c) TOC (% of dry weight sediment), (d)  $\delta^{13}\text{C}_{\text{org}}$  (% vs PDB), (e) IP<sub>25</sub> ( $\mu\text{g g}^{-1}$  TOC, black) and (f) ( $\mu\text{g g}^{-1}$  sediment (sed.), orange), (g) brassicasterol ( $\mu\text{g g}^{-1}$  TOC, black) and (h) ( $\mu\text{g g}^{-1}$  (i) calculated index P<sub>B</sub>IP<sub>25</sub> (brassicasterol), (j) dinosterol ( $\mu\text{g g}^{-1}$  black) and (k) ( $\mu\text{g g}^{-1}$ , (l) calculated index P<sub>D</sub>IP<sub>25</sub> (dinosterol), (m) relative abundance of diatom species *Fragilariopsis oceanica* (Cleve) Hasle (% blue), (n) relative abundance of diatom species *Thalassiosira oestrupii* (Ostenfeld) Hasle (% magenta), (o) diatom flux ( $10^{05}$  frustules (fr.) per  $\text{cm}^2$  per kyr, black) and (p) diatom concentrations ( $10^{05}$  frustules per g sed., orange), and MIS are shown. Vertical lines in IP<sub>25</sub>, brassicasterol and P<sub>B</sub>IP<sub>25</sub> mark the cutoff values of sea ice cover stages<sup>26,27</sup>. Legend at the bottom of the figure show cutoff values of IP<sub>25</sub> ( $\mu\text{g g}^{-1}$  TOC), brassicasterol ( $\mu\text{g g}^{-1}$  TOC) and P<sub>B</sub>IP<sub>25</sub> as criteria of the interpretation of IP<sub>25</sub>, brassicasterol, dinosterol, P<sub>B</sub>IP<sub>25</sub> and P<sub>D</sub>IP<sub>25</sub> in terms of degree of sea ice cover. Brassicasterol values (as proxy for open-water phytoplankton productivity) are in great accordance with the dinosterol numbers, therefore only values for brassicasterol are shown. Zero or near-zero concentrations of both IP<sub>25</sub> as well as phytoplankton biomarkers are indicative for a closed (spring) sea ice cover (PIP<sub>25</sub> in general is indeterminable and per definition set to '1' (refs 15,26); see P<sub>B</sub>IP<sub>25</sub> and P<sub>D</sub>IP<sub>25</sub> during H1, marked by blue stars). Arrows mark events of increased productivity during IS cooling phases (see text for explanation). H, H-event; 'not enough diatoms preserved', in these intervals there were not enough diatoms preserved to be quantified after the set criteria (see Methods).

sampling resolution in JM-FI-19PC in this time interval (>300 years per sample) not all the interstadials are equally well resolved (Fig. 5; see also ref. 30). In the following discussion we therefore focus on the time interval 90–35 kyr ago comprising the longer-lasting D/O events 21–7 with the highest resolution, including H-events H8–H4 (Fig. 5). A total of three different phases within each D/O event could be determined; interstadial conditions, interstadial transitional cooling conditions and stadial conditions

(Fig. 5). A fourth phase describes the particular conditions during some larger H-events (H6, part of H4 and H1; Fig. 5).

Interstadials are characterized by absence or near absence of IP<sub>25</sub>, maximum content of brassicasterol and dinosterol, and low P<sub>B</sub>IP<sub>25</sub> and P<sub>D</sub>IP<sub>25</sub> values (Fig. 5). The (near) absence of IP<sub>25</sub> indicates absence of sea ice-related diatoms, while high brassicasterol and dinosterol values indicate favourable conditions for phytoplankton growth in general and higher primary

productivity at the surface ocean. *Thalassiosira oestrupii* (Ostenfeld) Hasle, an indicator of relatively warm temperatures<sup>32,33</sup> is present in higher amounts in IS21 (MIS 5a) and in the Holocene, coinciding with high values of brassicasterol and dinosterol (Fig. 5, see Methods for details on diatoms). The species occurs sporadic or is absent in interstadials of MIS 3 and 2 (IS17–IS3) indicating colder than modern conditions. Altogether, the biomarker signals indicate open-ocean conditions and relatively high surface water temperatures over the northern Faroe Islands margin, with the Arctic Front located north of the core position (Fig. 6a). Planktic foraminiferal species from nearby core ENAM93-21/MD95-2009 indicated inflow of Atlantic Water during interstadials of MIS 3 and MIS 2<sup>3</sup> in support of the interpretation based on diatom floras and organic biomarkers. Furthermore, the  $\delta^{13}\text{C}_{\text{org}}$  values are higher in interstadials, which point to a (relative) decrease of terrigenous organic matter supply and/or an increase in marine organic matter input<sup>28</sup>. The latter option, that is, an increased influence of marine organic matter at times of higher water temperatures due to higher marine productivity at the core location, is supported by higher flux of diatoms and higher concentrations of brassicasterol and dinosterol (Figs 5 and 6a).

The optimum conditions are followed by a cooling phase defined by gradual changes to medium or higher values of  $\text{IP}_{25}$ , brassicasterol, and dinosterol,  $\text{P}_{\text{B}}\text{IP}_{25}$  and  $\text{P}_{\text{D}}\text{IP}_{25}$  (Fig. 5). The relatively higher  $\text{P}_{\text{B}}\text{IP}_{25}$  and  $\text{P}_{\text{D}}\text{IP}_{25}$  values together with the increase in brassicasterol and dinosterol values (most clearly seen in IS21, IS20, IS13–10 and IS8; marked by arrows in Fig. 5) indicate increasing seasonal sea ice cover and elevated surface productivity, respectively, typical of the marginal ice zone<sup>11,12</sup> (Fig. 6b). These findings suggest that the IFF had moved to a probably variable position south-east of the core location and that the area was in the zone of Arctic surface water, likely resulting in decrease of both atmospheric and surface-water temperatures (Fig. 6b). This phase correlates with an increase in ice rafting and an increase in cold-water planktic foraminiferal species as seen in nearby core ENAM93-21/MD95-2009 (ref. 3).

The cooling phase terminated in a phase of extended sea ice cover. This is associated with a maximum in  $\text{IP}_{25}$  values (higher than the calculated mean value), an abrupt decrease in the concentration of brassicasterol, dinosterol and high  $\text{P}_{\text{B}}\text{IP}_{25}$  and  $\text{P}_{\text{D}}\text{IP}_{25}$  values (Fig. 5, light-blue colour bars). Generally supporting this, the sea ice-associated *Fragilariopsis oceanica* (Cleve) Hasle<sup>33–35</sup> is present in higher relative abundance in H-event 8, S16 and S1 (Fig. 5, see Methods for details on diatoms). The lack of diatoms in most of the identified phases of extended sea ice cover (Fig. 5) is in accordance with the low abundances of diatoms found in areas with near-perennial sea ice cover today<sup>16,20</sup> (for diatom preservation, see Methods). With cold surface conditions and extended sea ice cover as far south as the core location, the Polar Front migrated to a position close to or probably south of the core site (Fig. 6c). Conditions were probably similar to conditions currently observed in areas governed by the East Greenland Current with (very) low primary productivity<sup>36,37</sup> and a dense pack-ice cover. Rather low  $\delta^{13}\text{C}_{\text{org}}$  values might indicate decreased marine organic carbon flux due to the low productivity and/or an increased influence of terrigenous organic matter, probably being ice-rafted to the core site. The presence of near-perennial sea ice prevented heat exchange and the atmosphere was probably very cold. These last phases of the D/O events represent the stadial conditions of the Greenland ice cores.

The sea ice proxy data for the H-events 6, 4 and 1 (Figs 4 and 5) show a very prominent period of perennial or near-perennial sea ice cover (absent or medium  $\text{IP}_{25}$ , respectively, absent

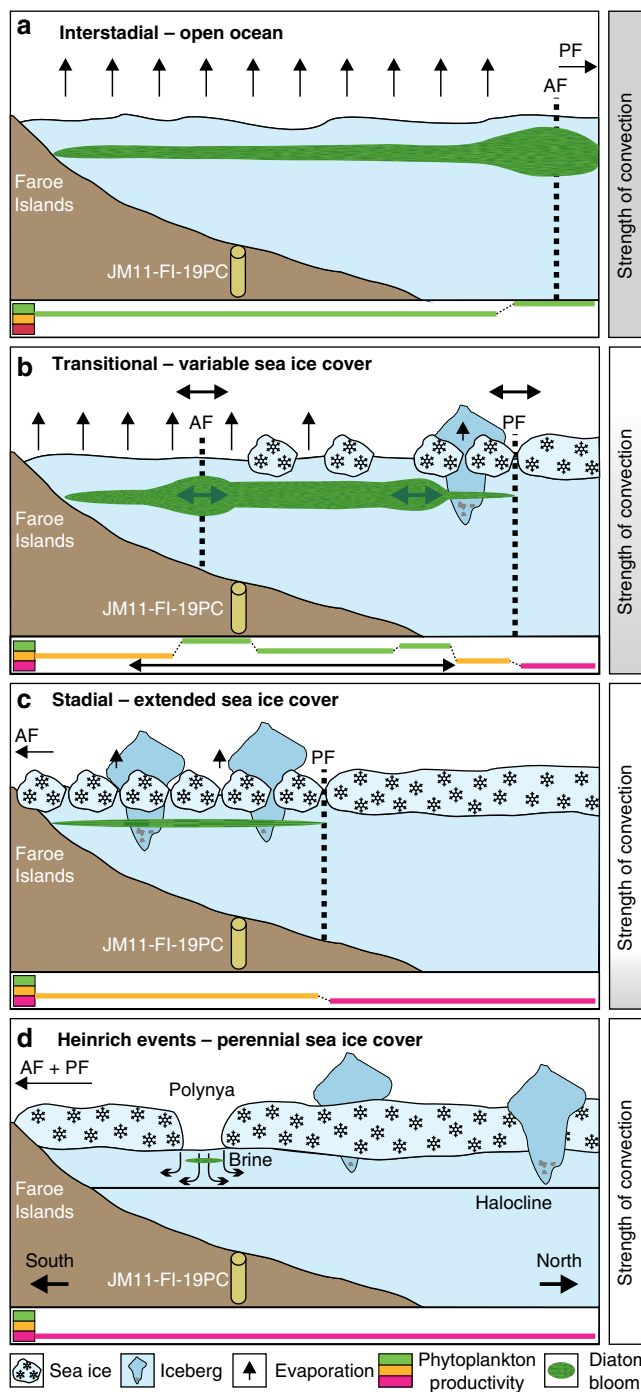


**Figure 6 | Schematic reconstruction of sea ice conditions at the northern Faroe slope. (a)** Interstadial. **(b)** Interstadial transitional cooling phase. **(c)** Stadial. **(d)** H-events H6, H4 and H1. Black horizontal arrows indicate location of the Arctic Front (AF) and Polar Front (PF). Green colour (including arrows) indicates degree of phytoplankton productivity inferred from concentrations of brassicasterol, dinosterol and flux of diatoms. Productivity levels are indicated in the lowermost part of each figure: Magenta coloured line, no or very little phytoplankton productivity; yellow line, medium/variable productivity; green line, high or very high productivity. Grey vertical bars on the right indicate strength of deep convection.

or minimal brassicasterol and dinosterol, and maximum  $\text{P}_{\text{B}}\text{IP}_{25}$  and  $\text{P}_{\text{D}}\text{IP}_{25}$  values). In these intervals, the  $\text{IP}_{25}$  values of zero cannot be interpreted as absence of sea ice. Instead, the combined signals likely represent a thick permanent sea ice cover and very cold

temperatures<sup>15,26</sup> (see also discussion in ref. 17). As long as the sea ice cover is thin enough for sunlight to penetrate, sea ice diatoms synthesizing IP<sub>25</sub> can grow attached beneath the ice<sup>14,16,20</sup>, which was probably the case at the beginning and end of some of the stadial intervals, where high peaks in P<sub>B</sub>IP<sub>25</sub> and P<sub>D</sub>IP<sub>25</sub> can occur (Fig. 5). When the sea ice becomes permanent and too thick for sunlight to penetrate, the signal of IP<sub>25</sub> will drop to zero (Fig. 5). To allow for the perennial sea ice and extreme cold temperatures, Polar surface water most likely spread over the area north of the Faroe Islands and the Polar Front was located far more southerly than today and during the smaller stadials (Fig. 6d).

The transition from stadial and H-events to interstadials is rapid and interpreted as a sudden transition from extended sea ice cover to open-ocean conditions, seen as a decrease in values of IP<sub>25</sub>, P<sub>B</sub>IP<sub>25</sub> and P<sub>D</sub>IP<sub>25</sub> (with the exception of H6, H4 and H1; Fig. 5). The abrupt decrease in sea ice cover is in line with the abrupt increase in atmospheric temperatures at the beginning of D/O events<sup>1</sup> and increase in sea surface temperatures as also seen in nearby record ENAM93-21/MD95-2009 (ref. 3).

Our data generally show a good correlation between climate and sea ice cover for MIS 3, as well as for the last 30,000 years (Figs 4 and 5). We demonstrate that the presence/absence of sea ice varies closely in pace with the different climatic phases of the D/O millennial-scale climate events (Fig. 5). The peak warm interstadials with no sea ice (Fig. 7a) (Supplementary Fig. 1 and Supplementary Table 1) resembled the modern conditions, which have been shown by numerous marine core studies from the northern North Atlantic and Nordic seas, and have generally been interpreted as a sign of strong flow of Atlantic surface water (Fig. 6a). The transitional cooling phase of the interstadial with gradually expanding sea ice cover from northwest (Figs 6b and 7b) correlate with increase in ice rafting from icebergs, decreasing atmospheric temperatures<sup>1</sup> and an increasing amount of meltwater over a larger area of the northern North Atlantic region and Nordic seas. In the following stadial events iceberg rafting reached a maximum (Figs 6c and 7c) as also seen in nearby core ENAM93-21/MD95-2009 and other records from the Nordic seas and North Atlantic (Supplementary Fig. 1 and Supplementary Table 1), and  $\delta^{18}\text{O}$  values reached very low values indicating presence of meltwater (Fig. 5). Sea ice advanced and the sea ice cover became near-perennial in the case of smaller stadial events (Figs 6c and 7c) or perennial as during the colder H-events H6, H4 and H1 (Figs 6d and 7d). The latter events are the three strongest events during the last 90 kyr, probably due to orbital forcing<sup>2,38</sup>. All stadial and H-events in the North Atlantic and Nordic seas show dominance by the polar planktic foraminifera *Neogloboquadrina pachyderma* sinistral (s) and cold polar conditions (see references in Supplementary Information; Supplementary Fig. 1 and Supplementary Table 1).

Sea ice was an active player in millennial climate change, in most cases probably enforcing trends already caused by the predominantly cold, glacial atmospheric conditions during the last glacial period. The peak warmth of the interstadials lasted only shortly<sup>1</sup> and was immediately followed by cooling and spreading of sea ice. The inflow of Atlantic surface Water to the core area diminished to the extent that deep-water formation became very slow and stopped and sea ice cover became perennial or near perennial. The ocean circulation in the Nordic seas was probably more similar to the system in the northern Fram Strait today, in our view the closest analogue to the situation during stadials and North Atlantic H-events<sup>38</sup> and with similar circulation patterns of water masses with warmer Atlantic water flowing at intermediate depth below Polar surface Water<sup>38–41</sup>. In other words, the present-day conditions of the Fram Strait moved far south into the Atlantic Ocean (Fig. 7c,d). The remarkable

abrupt disappearance of sea ice at the end of stadials/H-events correlates with sudden renewed inflow of Atlantic surface Water, peak interstadial warmth and probably onset of deep-water formation. The distribution of sea ice thus correlated closely with variations in ocean circulation and expanding-retreating ice sheets and variations in flow of meltwater and stratification of the ocean surface.

## Methods

**Core logging and sampling.** The core handling, sampling and diatom flora analyses of sediment core JM11-FI-19PC (62°49.97 N; 03°52.03 W; 1179 m water depth; 1109 cm core recovery) were performed at the Department of Geology, UiT, Arctic University of Norway, Tromsø, Norway. Before opening the magnetic susceptibility (MS) was measured with a Bartington MS meter MS2 (loop; sample resolution: 1 cm). After opening of the core, but before sampling, it was scanned for light and heavy elements, such as potassium (K) or titanium (Ti) with an Avaatech XRF core scanner in a resolution of 0.5–1 cm (ref. 30).

Samples taken at 5-cm intervals in 1-cm thick slices were weighed, freeze-dried and weighed again before wet sieving over 63 and 100- $\mu\text{m}$  sieves. Tephra particles were counted in the size fraction > 100  $\mu\text{m}$ . The method for counting tephra particles followed the procedures described in Wastegård and Rasmussen<sup>42</sup>.

Subsamples at 5-cm intervals from the presented core section (801–2 cm) were used to determine TOC. For %TOC dried and powdered aliquots of the samples were treated with 10% hydrochloric acid (HCl), for carbonate removal, before being measured with a Leco CS-200.

**Carbon isotopes of organic material.** Carbon isotopes  $\delta^{13}\text{C}_{\text{org}}$  were measured every 5 cm in a powdered and carbonate-free aliquot of the samples, using a Finnigan MAT Delta-S mass spectrometer equipped with a FLASH elemental analyser and a CONFLO III gas mixing system for the online determination of the carbon isotopic composition. Measurements were conducted at the Alfred Wegener Institute Helmholtz Centre for Polar and Marine Research in Potsdam, Germany. The s.d. ( $1\sigma$ ) is generally better than  $\delta^{13}\text{C} = \pm 0.15\%$ .

**Oxygen isotopes in planktic foraminifera.** Oxygen isotopes were measured on specimens of the planktic foraminiferal species *N. pachyderma* s. For this, about 30 specimens in the size fraction 150–250  $\mu\text{m}$  were analysed with a Finnigan MAT 251 mass spectrometer with an automated carbonate preparation device. Measurements were performed at the Department of Geosciences, at the University of Bremen, Germany. The external standard error of the oxygen isotope analyses is  $\delta^{18}\text{O} = \pm 0.07\%$ . Values are reported relative to the Vienna Pee Dee Belemnite, and calibrated by using the National Bureau of Standards NBS18, 19 and 20.

**Quantification of diatom floras.** The preparation method for diatom samples given in Koç *et al.*<sup>43</sup> was followed, but using hydrogen peroxide (H<sub>2</sub>O<sub>2</sub> 37%; 10 drops) instead of nitric acid (HNO<sub>3</sub> 65%) to remove existing organic matter around the diatom valves. Quantitative diatom slides were produced as described in Koç Karpuz and Schrader<sup>44</sup>. A sample was considered to contain enough diatoms for quantification, when there were more than 40 diatom valves (= 20 frustules) within ~350 fields of view (2 vertical transects) and a minimum of 300 diatom valves per sample were counted. A total of 52 species that previously have been used by Koç Karpuz and Schrader<sup>44</sup> for establishing a sea-surface-temperature-transfer function (including additional species added by Andersen *et al.*<sup>45</sup>) have been identified and counted on a *Chaetoceros* spp. free basis<sup>44,46</sup>. Diatom counts followed the procedures of Schrader and Gersonde<sup>47</sup> and taxonomic identification mainly followed those of Hustedt<sup>48,49</sup>, Fryxell and Hasle<sup>50,51</sup>, Simonsen<sup>52</sup>, Hasle and Fryxell<sup>53</sup>, Hasle<sup>54</sup>, Syvertsen<sup>55</sup>, Sancetta<sup>56</sup> and Sundström<sup>57</sup>.

For the interval between 78 and ~15 kyr b2k numerous fragmented frustules were found. This might indicate that this interval was influenced by dissolution processes<sup>58</sup>, which additionally could have altered the species composition of the diatom flora, and/or, that the sediments were directly influenced by the presence of sea ice as a mechanical component, breaking diatom valves by shear forces<sup>59</sup>. Diatom data for this interval have thus to be considered with caution and our reconstruction of past sea ice cover is exclusively based on the biomarker proxies that are more resistant and preserved in this type of sediments<sup>14,16,23</sup> (for general aspects of preservation of biomarkers see refs 28,60). Between ~15 kyr b2k and the present the preservation of diatom frustules is excellent.

**Biomarker analyses.** The lipid biomarker analyses were performed at the Alfred Wegener Institute Helmholtz Centre for Polar and Marine Research, Bremerhaven, Germany. Freeze-dried and homogenized sediments (4–5 g) were extracted with an Accelerated Solvent Extractor (DIONEX, ASE 200; 100 °C, 5 min, 1000 psi) using a dichloromethane:methanol mixture (2:1 v/v). Before this step, 7-hexylnonadecane, squalane and cholesterol-*d*<sub>6</sub> (cholest-5-en-3 $\beta$ -ol-*d*<sub>6</sub>) were added as internal standards. Hydrocarbons and sterols were separated via open column chromatography

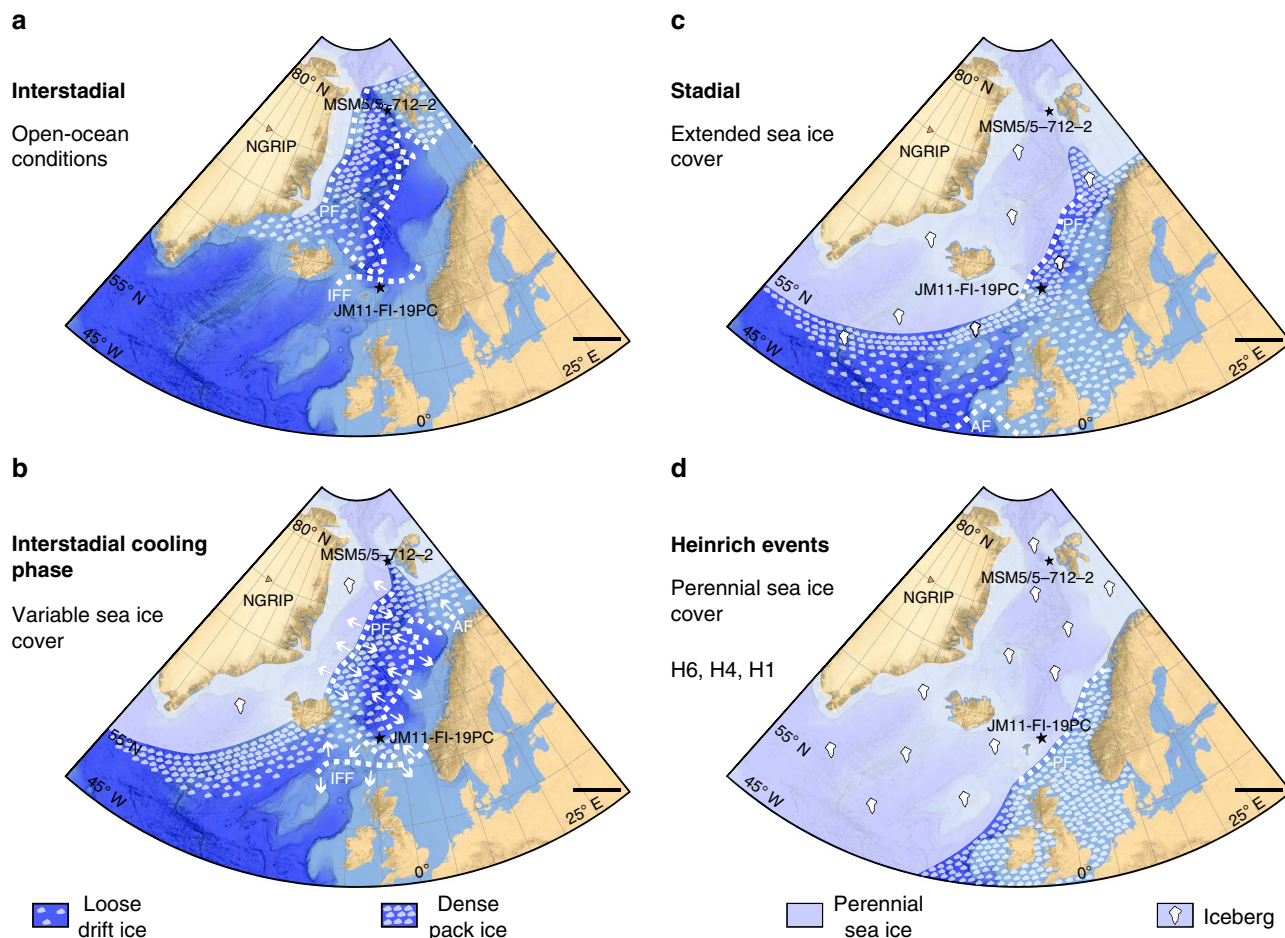


**Figure 7 | Reconstructed sea ice distribution during D/O events in the Nordic seas.** The figure is based on published records with sufficient time resolution to identify individual D/O events of MIS 5 to MIS 2. We have included only records that contain counts of ice-rafted debris (IRD) in combination with planktic  $\delta^{18}\text{O}$  values and/or surface temperature proxies based on planktic foraminifera (transfer functions and/or % *N. pachyderma*). From areas that are well covered with a high number of records, we have selected a few considered as representative. For areas with sparse coverage and low resolution (such as central basins), we chose a few records, where the results may be based on other or fewer proxies (Supplementary Table 1). For locations of the published records and references, see Supplementary Fig. 1. **(a)** Interstitial with open-ocean conditions. The Arctic Front (AF), Iceland-Faroe Front (IFF) and Polar Front (PF) are located north of the core location. **(b)** Interstitial transitional cooling phase with variable sea ice cover and variable positions of AF (IFF) and PF, which is indicated by white arrows. The core location is always between AF and PF. **(c)** Stadial with extended sea ice cover. The core location is again between AF and PF, but markedly closer to PF (potentially PF can be south of the core location; see text). Both fronts are located further towards the south compared with interstitial and interstitial cooling conditions. **(d)** H-events (H6, H4 and H1) with perennial sea ice cover. Both Fronts, AF and PF, are now located south of the core location. Stars mark the location of the studied core JM11-FI-19PC, as well as the location of core MSM5/5-712-2<sup>17</sup> used for comparison; dashed white lines give approximate positions of fronts AF (IFF) and PF. The reconstructions of regional distribution of sea ice cover are based on published records together with the records of JM11-FI-19PC and MSM5/5-712-2<sup>17</sup> (Supplementary Fig. 1, Supplementary Table 1 and Supplementary References). Bathymetry from GEBCO 2014 grid (<http://www.gebco.net/>). NGRIP, North Grip ice core (orange triangle). Scale bar, 500 km.

( $\text{SiO}_2$ ) using *n*-hexane (5 ml) and methyl-acetate:*n*-hexane (20:80 v/v, 6 ml), respectively. Sterols were silylated with 500  $\mu\text{l}$  BSTFA (60 °C, 2 h)<sup>61</sup>. For qualification and quantification of IP<sub>25</sub> and sterols see Fahl and Stein<sup>62</sup>. The detection limit for IP<sub>25</sub> is 0.01 ng on column. P<sub>B</sub>IP<sub>25</sub> and P<sub>T</sub>IP<sub>25</sub> were calculated from IP<sub>25</sub>, brassicasterol and dinosterol concentrations, respectively, according to Müller *et al.*<sup>26</sup>.

It is important, when using the PIP<sub>25</sub> index to distinguish between different sea ice conditions, that coevally high amounts of both biomarkers (suggesting ice-edge conditions) as well as coevally low contents (suggesting permanent-like ice conditions) would give a similar or even the same PIP<sub>25</sub> value. Especially, for the latter situation of permanent sea ice conditions both biomarker concentrations may approach values around zero and the PIP<sub>25</sub> index may become indeterminate (or misleading). For a correct interpretation of the PIP<sub>25</sub> data the individual IP<sub>25</sub> and phytoplankton biomarker concentrations must be considered<sup>15,26</sup>. Recently, Smik *et al.*<sup>63</sup> introduced a HBI-III alkene as phytoplankton biomarker replacing the sterols in the PIP<sub>25</sub> calculation. This modified PIP<sub>25</sub> approach is based on biomarkers from the same group of compounds (that is, HBIs) with more similar diagenetic sensitivity, which is important for palaeo-sea ice reconstructions and comparison of records from different Arctic areas.

**Radiocarbon dating.** Eleven AMS-<sup>14</sup>C dates of piston core JM11-FI-19PC have previously been presented by Ezat *et al.*<sup>30</sup>. They were performed on monospecific samples of the planktic foraminiferal species *N. pachyderma* s (Supplementary Table 3). Measurements were performed at the <sup>14</sup>CHRONO Centre for Climate, the Environment, and Chronology, at Queens University Belfast, Northern Ireland. For this study all <sup>14</sup>C ages were calibrated to calendar years using the CALIB Radiocarbon Calibration 7.0.2. software and the Marine13 data set (including 400 year correction for surface reservoir ages)<sup>64,65</sup>. To make the age scale comparable to the ice core timescale (GICC05) 50 years were added. All ages are in ice core years b2k (before year AD 2000).

**Construction of the age model.** The age model younger than 65 kyr is based on the age model published in Ezat *et al.*<sup>30</sup>. The age model from 90 to 65 kyr b2k was constructed by using the same approach and at the same time validating the age model of the younger sediments published by Ezat *et al.*<sup>30</sup> (Supplementary Tables 2, 3 and 4). To further solidify the age model, piston core JM11-FI-19PC was not only correlated to the NGRIP ice core but also to the nearby compiled marine cores ENAM93-21 (ref. 3) and MD95-2009 (refs 66,67) based on the



MS, common tephra layers and stable oxygen isotopes ( $\delta^{18}\text{O}$ ) measured in the planktic foraminiferal species *N. pachyderma* s (Fig. 2; see also Supplementary Table 2). The ages in between the tie points and/or tephra layers were calculated by interpolation assuming a constant sedimentation rate (Fig. 3).

**Data availability.** Data referenced in this study are available in PANGAEA with the identifier DOI 'https://doi.org/10.1594/PANGAEA.859992'.

## References

- Dansgaard, W. *et al.* Evidence for general instability of past climate from a 250-kyr ice-core record. *Nature* **364**, 218–220 (1993).
- Bond, G. *et al.* Correlations between climate records from North Atlantic sediments and Greenland ice. *Nature* **365**, 143–147 (1993).
- Rasmussen, T. L., Thomsen, E., Labeyrie, L. & van Weering, T. C. E. Circulation changes in the Faeroe-Shetland Channel correlating with cold events during the last glacial period (58–10 ka). *Geology* **24**, 937–940 (1996).
- Ruddiman, W. F. Late Quaternary deposition of ice-rafted sand in the subpolar North Atlantic (lat 40° to 65°N). *Geol. Soc. Am. Bull.* **88**, 1813–1827 (1977).
- Heinrich, H. Origin and consequences of cyclic ice rafting in the northeast Atlantic Ocean during the last 130,000 years. *Quat. Res.* **29**, 142–152 (1988).
- Hansen, B. & Østerhus, S. North Atlantic-Nordic seas exchanges. *Prog. Oceanogr.* **45**, 109–208 (2000).
- Aagaard, K., Foldvik, A. & Hillman, S. R. The West Spitsbergen Current: disposition and water mass transformation. *Geophys. Res.* **92**, 3778–3784 (1987).
- Li, C., Batisti, D. S. & Bitz, C. M. Can North Atlantic sea-ice anomalies account for Dansgaard-Oeschger climate signals? *J. Clim.* **23**, 5457–5475 (2010).
- Petersen, S. V., Schrag, D. P. & Clark, P. U. A new mechanism for Dansgaard-Oeschger cycles. *Paleoceanography* **23**, 1–7 (2013).
- Deser, C. & Teng, H. Evolution of Arctic sea-ice concentration trends and the role of atmospheric circulation forcing, 1979–2007. *Geophys. Res. Lett.* **35**, L02504 (2008).
- Smith, S. L., Smith, W. O., Codispodi, L. A. & Wilson, D. L. Biological observations in the marginal ice zone of the East Greenland Sea. *J. Mar. Res.* **43**, 693–717 (1985).
- Reigstad, M., Carroll, J., Slagstad, D., Ellingsen, I. & Wassmann, P. Intra-regional comparison of productivity, carbon flux and ecosystem composition within the northern Barents Sea. *Prog. Oceanogr.* **90**, 33–46 (2011).
- Rippeth, T. P. *et al.* Tide-mediated warming of Arctic halocline by Atlantic heat fluxes over rough topography. *Nat. Geosci.* **8**, 191–194 (2015).
- Belt, S. T. *et al.* A novel chemical fossil of palaeo sea ice: IP<sub>25</sub>. *Org. Geochem.* **38**, 16–27 (2007).
- Stein, R., Fahl, K. & Müller, J. Proxy reconstruction of Cenozoic Arctic Ocean sea-ice history -From IRD to IP<sub>25</sub>-. *Polarforschung* **82**, 37–71 (2012).
- Belt, S. T. & Müller, J. The Arctic sea-ice biomarker IP<sub>25</sub>: a review of current understanding, recommendations for future research and applications in palaeo sea-ice reconstructions. *Quat. Sci. Rev.* **79**, 9–25 (2013).
- Müller, J. & Stein, R. High-resolution record of late glacial and deglacial sea ice changes in Fram Strait corroborates ice-ocean interactions during abrupt climate shifts. *Earth Planet. Sci. Lett.* **403**, 446–455 (2014).
- Cabedo-Sanz, P., Belt, S. T., Knies, J. & Humus, K. Identification of contrasting seasonal sea ice conditions during the Younger Dryas. *Quat. Sci. Rev.* **79**, 74–86 (2013).
- Weckström, K. *et al.* Evaluation of the sea ice proxy IP<sub>25</sub> against observational and diatom proxy data in the SW Labrador Sea. *Quat. Sci. Rev.* **79**, 53–62 (2013).
- Brown, T. A., Belt, S. T., Tatarek, A. & Mundy, C. J. Source identification of the Arctic sea ice proxy IP<sub>25</sub>. *Nat. Commun.* **5**, 4197 (2014).
- Stein, R. & Fahl, K. Biomarker proxy IP<sub>25</sub> shows potential for studying entire Quaternary Arctic sea-ice history. *Org. Geochem.* **55**, 98–102 (2013).
- Knies, J. *et al.* The emergence of modern sea ice cover in the Arctic Ocean. *Nat. Commun.* **5**, 1–5 (2014).
- Stein, R. *et al.* Evidence for ice-free summers in the late Miocene central Arctic Ocean. *Nat. Commun.* **7**, 11148 (2016).
- De Vernal, A., Gersonde, R., Goose, H., Seidenkrantz, M.-S. & Wolff, E. W. Sea ice in the paleoclimate system: the challenge of reconstructing sea ice from proxies—an introduction. *Quat. Sci. Rev.* **79**, 1–8 (2013).
- Müller, J., Massé, G., Stein, R. & Belt, S. T. Variability of sea-ice conditions in the Fram Strait over the past 30,000 years. *Nat. Geosci.* **2**, 772–776 (2009).
- Müller, J. *et al.* Towards quantitative sea ice reconstructions in the northern North Atlantic: a combined biomarker and numerical modelling approach. *Earth Planet. Sci. Lett.* **306**, 137–148 (2011).
- Xiao, X., Fahl, K., Müller, J. & Stein, R. Sea-ice distribution in the modern Arctic Ocean: biomarker records from trans-Arctic Ocean surface sediments. *Geochim. Cosmochim. Acta* **155**, 16–29 (2015).
- Meyers, P. A. Organic geochemical proxies of paleoceanographic, paleolimnologic and paleoclimatic processes. *Org. Geochem.* **27**, 213–250 (1997).
- Lamb, H. H. Climatic variation and changes in the wind and ocean circulation: the Little Ice Age in the Northeast Atlantic. *Quat. Res.* **11**, 1–20 (1979).
- Ezat, M. M., Rasmussen, T. L. & Groeneveld, J. Persistent intermediate water warming during cold stadials in the southeastern Nordic seas during the past 65 k.y. *Geology* **42**, 663–666 (2014).
- Rasmussen, T. L., Balbon, E., Thomsen, E., Labeyrie, L. & Van Weering, T. C. E. Climate records and changes in deep outflow from the Norwegian Sea ~150–55 ka. *Terra Nova* **11**, 61–66 (1999).
- Maynard, N. G. Relationship between diatoms in surface sediments of the Atlantic Ocean and the biological and physical oceanography of overlying waters. *Paleobiology* **2**, 99–121 (1976).
- Sha, L. *et al.* A diatom-based sea-ice reconstruction for the Vaigat Strait (Disko Bugt, West Greenland) over the last 5000yr. *Palaeogeogr. Palaeoclim.* **Palaeoecol.** **403**, 66–79 (2014).
- Jiang, H., Seidenkrantz, M.-S., Knudsen, K. L. & Eiriksson, J. Late-Holocene summer sea-surface temperatures based on a diatom record from the north Icelandic shelf. *Holocene* **12**, 137–147 (2002).
- Justwan, A. & Koç, N. A diatom based transfer function for reconstructing sea ice concentrations in the North Atlantic. *Mar. Micropaleontol.* **66**, 264–278 (2008).
- Huber, R., Meggers, H., Baumann, K.-H. & Heinrich, R. Recent and Pleistocene carbonate dissolution in sediments of the Norwegian-Greenland Sea. *Mar. Geol.* **165**, 123–136 (2000).
- Sakshaug, E. in *The Organic Carbon Cycle in the Arctic Ocean* (eds Stein, R. & Macdonald, R.W.) 57–82 (Springer, 2004).
- Rasmussen, T. L. & Thomsen, E. The role of the North Atlantic Drift in the millennial timescale glacial climate fluctuations. *Palaeogeogr. Palaeoclim.* **Palaeoecol.** **210**, 101–116 (2004).
- Shaffer, G., Olsen, S. M. & Bjerrum, C. J. Ocean subsurface warming as a mechanism for coupling Dansgaard-Oeschger climate cycles and ice-rafting events. *Geophys. Res. Lett.* **31**, L24202 (2004).
- Flückiger, J., Knutti, R. & White, J. W. C. Oceanic processes as potential trigger and amplifying mechanisms for Heinrich events. *Paleoceanography* **21**, PA2014 (2006).
- Marcott, S. A. *et al.* Ice-shelf collapse from subsurface warming as a trigger for Heinrich events. *Proc. Natl Acad. Sci. USA* **108**, 13415–13419 (2011).
- Wastegård, S. & Rasmussen, T. L. New tephra horizons from Oxygen Isotope Stage 5 in the North Atlantic: correlation potential for terrestrial, marine and ice-core archives. *Quat. Sci. Rev.* **20**, 1587–1593 (2001).
- Koç, N., Jansen, E. & Hafliðason, H. Paleoceanographic reconstructions of surface ocean conditions in the Greenland, Iceland and Norwegian seas through the last 14ka based on diatoms. *Quat. Sci. Rev.* **12**, 115–140 (1993).
- Koç Karpuz, N. & Schrader, H. Surface sediment diatom distribution and Holocene paleotemperature variations in the Greenland, Iceland and Norwegian Sea. *Paleoceanography* **5**, 557–580 (1990).
- Andersen, C., Koç, N., Jennings, A. & Andrews, J. T. Nonuniform response of the major surface currents in the Nordic seas to insolation forcing: implications for the Holocene climate variability. *Paleoceanography* **19**, PA2003 (2004).
- Miettinen, A., Koç, N., Hall, I. R., Godtlielsen, F. & Divine, D. North Atlantic sea surface temperatures and their relation to the North Atlantic Oscillation during the last 230 years. *Clim. Dyn.* **36**, 533–543 (2011).
- Schrader, H. & Gersonde, R. Diatoms and silicoflagellates. *Utrecht Micropal. Bull.* **17**, 129–176 (1978).
- Hustedt, F. in *Kryprogamenflora von Deutschland, Österreich und der Schweiz, Teil 1* (ed. Rabenhorst, L.) 1–920 (Akademische, 1930).
- Hustedt, F. in *Kryprogamenflora von Deutschland, Österreich und der Schweiz, Teil 2* (ed. Rabenhorst, L.) 1–845 (Akademische, 1959).
- Fryxell, G. A. & Hasle, G. R. *Thalassiosira eccentrica* (Ehrenb.) Cleve, *T. symmetrica* sp. nov., and some related centric diatoms. *J. Phycol.* **8**, 297–317 (1972).
- Fryxell, G. A. & Hasle, G. R. The marine diatom *Thalassiosira oestrupii*: structure, taxonomy and distribution. *Am. J. Bot.* **67**, 804–814 (1980).
- Simonsen, R. The diatom plankton of the Indian Ocean Expedition of R. V. *Meteor* 1964-1965. *Meteor Forschungsgergeb. Reihe D* **19**, 1–66 (1974).
- Hasle, G. R. & Fryxell, G. A. The genus *Thalassiosira*: some species with a linear areola array. *Nova Hedwigia* **54**, 15–66 (1977).
- Hasle, G. R. Some *Thalassiosira* species with one central process (Bacillariophyceae). *Norw. J. Bot.* **25**, 77–110 (1978).

55. Syvertsen, E. E. Resting spore formation in clonal cultures of *Thalassiosira antarctica* Comber, *Ts. nordenskoldii* Cleve and *Detonula confervacea* (Cleve) Gran. *Nova Hedwigia* **64**, 41–63 (1979).
56. Sancetta, C. Distribution of diatom species in surface sediments of the Bering and Okhotsk seas. *Micropaleontology* **28**, 221–257 (1982).
57. Sundström, B. G. *The Marine Diatom Genus Rhizosolenia*. PhD thesis. Univ. Lund (1986).
58. Ryves, D. B., Battarbee, R. W. & Fritz, S. C. The dilemma of disappearing diatoms: incorporating diatom dissolution data into palaeoenvironmental modeling and reconstruction. *Quat. Sci. Rev.* **28**, 120–136 (2009).
59. Scherer, R. P., Sjunneskog, C. M., Iverson, N. R. & Hooyer, T. S. Assessing subglacial processes from diatom fragmentation patterns. *Geology* **32**, 557–560 (2004).
60. Eglinton, T. I. & Eglinton, G. Molecular proxies for paleoclimatology. *Earth Planet. Sci. Lett.* **275**, 1–116 (2008).
61. Fahl, K. & Stein, R. Biomarkers as organic-carbon-source and environmental indicators in the Late Quaternary Arctic Ocean: problems and perspectives. *Mar. Chem.* **63**, 293–309 (1999).
62. Fahl, K. & Stein, R. Modern seasonal variability and deglacial/Holocene change of central Arctic Ocean sea-ice cover: new insights from biomarker proxy records. *Earth Planet. Sci. Lett.* **351–352C**, 123–133 (2012).
63. Smik, L., Cabedo-Sanz, P. & Belt, S. T. Semi-quantitative estimates of paleo Arctic sea ice concentration based on source-specific highly branched isoprenoid alkenes: a further development of the PIP25 index. *Org. Geochem.* **92**, 63–69 (2016).
64. Stuiver, M. & Reimer, P. J. Extended <sup>14</sup>C database and revised CALIB radiocarbon calibration program. *Radiocarbon* **35**, 215–230 (1993).
65. Reimer, P. J. *et al.* IntCal13 and Marine13 radiocarbon age calibration curves, 0–50,000 years cal BP. *Radiocarbon* **55**, 1869–1887 (2013).
66. Rasmussen, T. L., Thomsen, E. & Van Weering, T. C. E. Cyclic sedimentation on the Faeroe Drift 53–10 ka BP related to climatic variations. *Geol. Soc. Spec. Publ.* **129**, 255–267 (1998).
67. Rasmussen, T. L. *et al.* Stratigraphy and distribution of tephra layers in marine sediment cores from the Faeroe Islands, North Atlantic. *Mar. Geol.* **199**, 263–277 (2003).
68. Rasmussen, T. L., Thomsen, E., Kuijpers, A. & Wastegård, S. Late warming and early cooling of the sea surface in the Nordic seas during MIS 5e (Eemian Interglacial). *Quat. Sci. Rev.* **22**, 809–821 (2003).
69. Svensson, A. *et al.* A 60,000 year Greenland stratigraphic ice core chronology. *Clim. Past* **4**, 47–57 (2008).
70. Wolff, E. W., Chappellaz, J., Blunier, T., Rasmussen, S. O. & Svensson, A. Millennial-scale variability during the last glacial: the ice core record. *Quat. Sci. Rev.* **29**, 2828–2838 (2010).

## Acknowledgements

This research was supported by UiT, The Arctic University of Norway, the Mohn Foundation to the ‘Paleo-CIRCUS’ project, and part of the Centre of Excellence: Arctic Gas hydrate, Environment and Climate (CAGE) funded by the Norwegian Research Council (grant no. 223259). We thank the captain and crew of RV *Jan Mayen* for technical assistance in retrieving the sediment core. Matthias Forwick (UiT) is thanked for running the XRF-scanner and processing of the XRF-data. We thank Sunil Vadakkepuliambatta (UiT, CAGE) for assistance in producing the maps, and Nalan Koç (Norwegian Polar Institute) for reading an earlier version of the manuscript. Additional thanks go to Hanno Meyer (Alfred Wegener Institute Helmholtz Centre for Polar and Marine Research (AWI Potsdam)) for measuring the  $\delta^{13}\text{C}$ , and Walter Luttmer (AWI Bremerhaven) for technical assistance. We thank Simon Belt (Biogeochemistry Research Centre, University of Plymouth/UK) for providing the 7-HND standard for IP<sub>25</sub> quantification.

## Author contributions

U.H. sampled the core, counted and identified the diatom flora, assisted in constructing the age model and drafted the original manuscript; T.L.R. led the study and contributed substantially to all aspects; R.S. and K.F. were responsible for the biomarker analyses, evaluation and quality control; M.M.E. provided the oxygen isotope records and constructed the age model. All authors interpreted the results and contributed to the final manuscript.

## Additional information

**Supplementary Information** accompanies this paper at <http://www.nature.com/naturecommunications>

**Competing interests statement:** The authors declare no competing financial interests.

**Reprints and permission** information is available online at <http://npg.nature.com/reprintsandpermissions/>

**How to cite this article:** Hoff, U. *et al.* Sea ice and millennial-scale climate variability in the Nordic seas 90 kyr ago to present. *Nat. Commun.* **7**:12247 doi: 10.1038/ncomms12247 (2016).



This work is licensed under a Creative Commons Attribution 4.0 International License. The images or other third party material in this article are included in the article’s Creative Commons license, unless indicated otherwise in the credit line; if the material is not included under the Creative Commons license, users will need to obtain permission from the license holder to reproduce the material. To view a copy of this license, visit <http://creativecommons.org/licenses/by/4.0/>

© The Author(s) 2016